Plasma 2
Lecture 14:
Introduction to Low-Frequency Fluctuations and Transport

APPH E6102y

Columbia University

Gaseous Diffusion

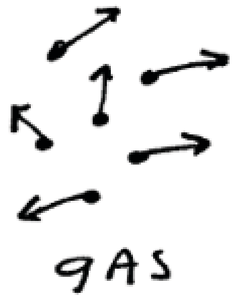

$$\frac{\partial n}{\partial t} = -\nabla \cdot \Gamma \qquad \Gamma = -D \frac{\partial n}{\partial x}$$

$$D = \lim_{t \to \infty} \frac{\langle (x(t) - x(0))^2 \rangle}{2t}$$

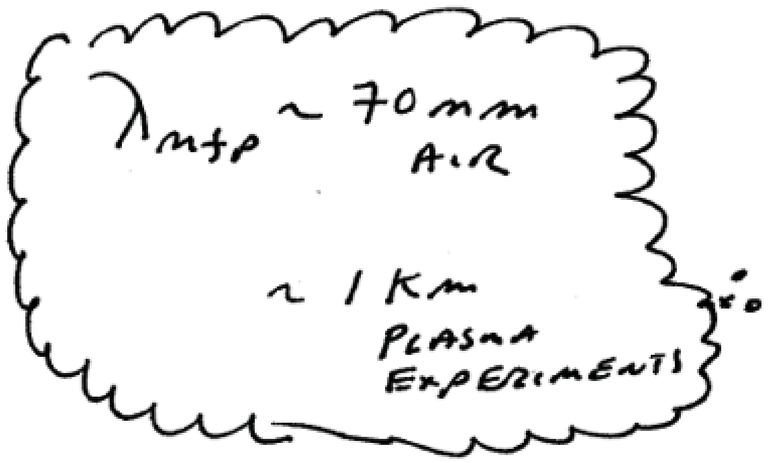

$$x(t) - x(0) = \int_0^t dt' V(t')$$

$$D = \int_0^\infty dt' \langle V(t') V(0) \rangle$$

$$= \langle v^2 \rangle \tau_{collision}$$

$\Longrightarrow$ MORE COLLISIONS, THEN <u>LESS</u> DIFFUSION

$$D \propto \frac{1}{\text{PRESSURE}}$$

(Classical) Diffusion in a Magnetized Plasma

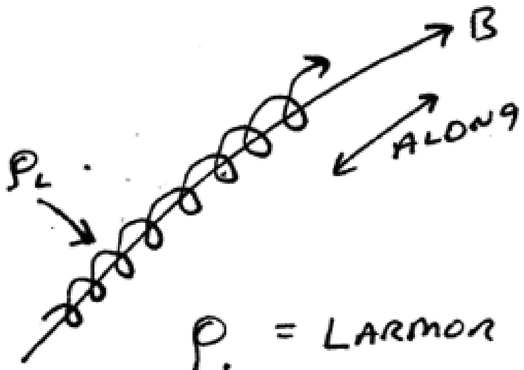

$D_{\parallel} \sim \langle v^2 \rangle \tau_{COL} \sim 10^{12} D_{\perp}$

ρ_L = LARMOR RADIUS $= \frac{v}{\omega_c}$

$\omega_c \sim \frac{eB}{m} \gg \frac{1}{\tau_{COLLISON}}$

MAGNITIZED

$D_{\perp} \sim \lim_{t \to \infty} \frac{\langle (x(t) - x(0))^2 \rangle}{2t}$

$|x(t) - x(0)| \sim \rho_L \sim$ RANDOM COLLISION STEP SIZE

$\therefore \quad D_{\perp} \sim \frac{\rho_L^2}{\tau_{COL}}$

MORE COLLISIONS, THEN MORE DIFFUSION

BUT $D_{\perp} \propto \frac{1}{B^2}$ ← SAME

Three Great Physicists

Winston H. Bostick (1916 - 1991)
Stevens Institute of Technology

Nat Rynn (1923 – 2017)
Princeton and UC-Irvine

Bo Lehnert (1926-)
Royal Inst. Technology Sweden

Experiments on the Behavior of an Ionized Gas in a Magnetic Field*

WINSTON H. BOSTICK AND MORTON A. LEVINE
Tufts College, Medford, Massachusetts

(Received March 15, 1954; revised manuscript received June 24, 1954)

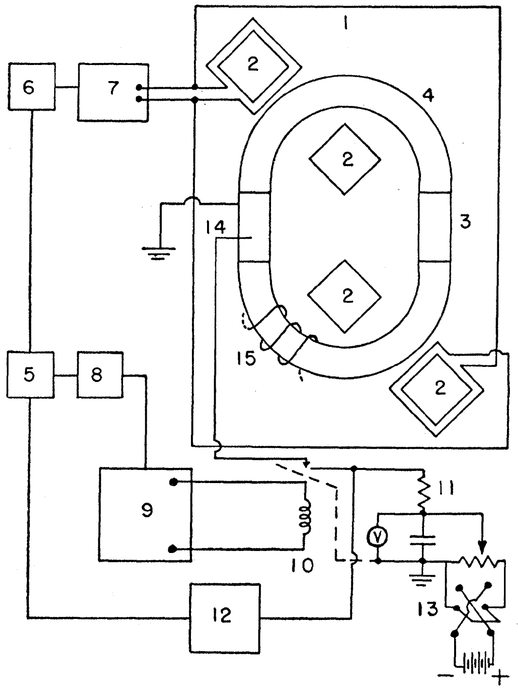

FIG. 1. Circuit used for induction-excitation of the toroidal discharge tube and measurement of ion density in the afterglow by means of a probe: (1) induction-excited toroid, (2) pulse transformer cores, (3) straight brass sections, (4) glass U bends, (5) master trigger source, (6) trigger amplifier, (7) pulse generator, 0.02 μf charged to 20 kv, (8) variable trigger delay, (9) pulse generator for relay coil, (10) Stevens-Arnold relay, (11) signal resistor for measuring positive-ion or electron current, (12) synchroscope, (13) dc voltage source for probe, (14) probe, and (15) coils for annular magnetic field.

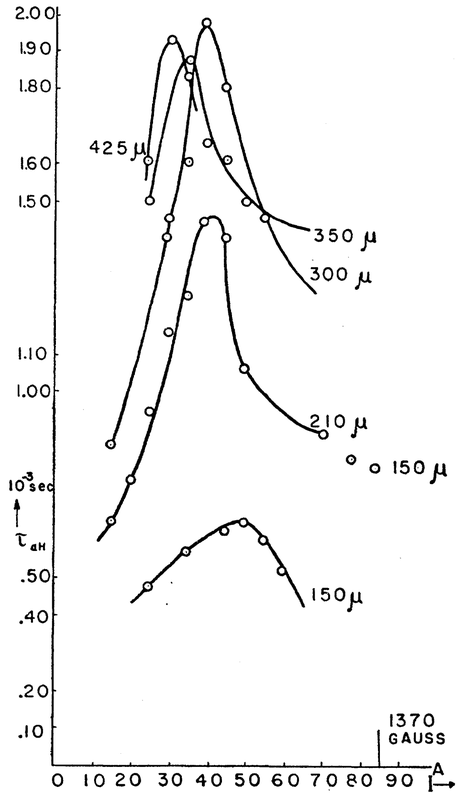

FIG. 8. Results of measurements of diffusion of He ions in helium gas in a toroid with an annular magnetic field. Ordinates are the decay times τ_{aH} which are proportional to $1/D_{aH}$, where D_{aH} is the ambipolar diffusion coefficient in a magnetic field. Abscissa is the magnetic field currents.

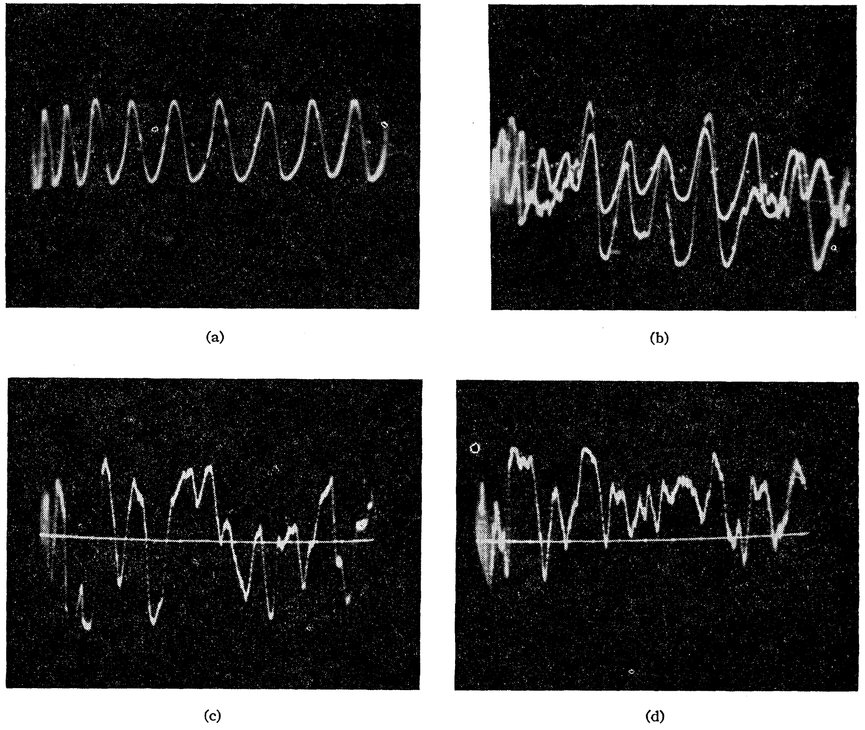

FIG. 2. (a) Argon at 0.5 mm Hg, $H=350$ gauss; frequency of oscillations is 6500 cps. (b) Argon at 0.5 mm Hg, $H=460$ gauss, $H=530$ gauss. (c) Argon at 0.2 mm Hg, $H=530$ gauss. (d) Argon at 0.2 mm Hg, $H=690$ gauss.

Current wave forms picked up by a probe in a plasma produced in the toroid shown in Fig. 1 at the indicated values of pressure and magnetic field in argon gas. The gas is excited by a dc potential of 600 volts between two probes which are diametrically opposite across the toroid. These wave forms are attributed to plasma waves of the magneto-hydrodynamic type. Note increase in higher-frequency components with increase in the magnetic field. Time is the abscissa and time marker dots are 100 μsec apart.

Diffusion Processes in a Plasma Column in a Longitudinal Magnetic Field

F. C. Hoh and B. Lehnert
Royal Institute of Technology, Stockholm, Sweden
(Received March 18, 1960)

3. EXPERIMENTAL ARRANGEMENT

The apparatus consists of a long discharge tube placed inside a magnetic coil, which is 3.5 m long and yields a maximum field of 0.9 v/m^2. Discharges were run with helium, argon, krypton, and hydrogen in a pressure range from about 0.1 to about 4 mm Hg and with discharge currents up to 1 amp. The cathode and the anode are situated at the tube ends which are extended each some 0.25 m outside the ends of the coil. Experiments were performed with three tube radii, $R = 0.535$, 0.76, and 1.00 cm. Two probes at the tube wall about 0.4 m apart and connected over an electrostatic voltmeter served to indicate the longitudinal electric field. A detailed description of the apparatus and the techniques used will be given elsewhere together with a discussion of the experimental conditions.[21]

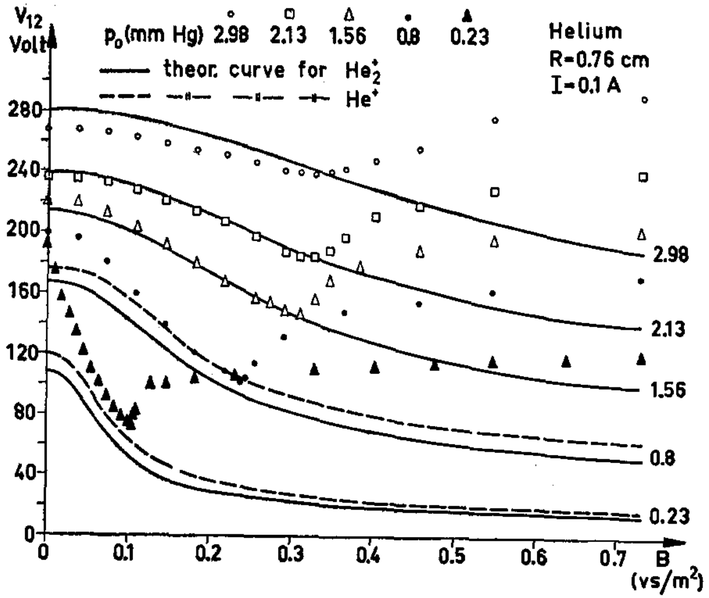

FIG. 3. Voltage drop measured across two probes 0.345 m apart as a function of the magnetic field. The full curves are calculated from the theory for molecular ions and the dashed curves for atomic ions.

5. CONCLUSIONS

The results obtained in this paper confirm the conclusions drawn in earlier investigations,[5,22] about the diffusion processes in a magnetic field. The abnormal behavior of the electric field characteristics above a certain magnetic field is a phenomenon which exists also in other gases than helium. This

The phenomena described in this paper and earlier investigations on diffusion[5,6,22] are likely to be intimately related to the rapid particle losses observed in the B-3 Stellarator of Project Matterhorn which may be due to some enhanced diffusion across the magnetic field.[8]

Improved Quiescent Plasma Source*

NATHAN RYNN
Plasma Physics Laboratory, Princeton University, Princeton, New Jersey

(Received 20 August 1963; and in final form, 3 October 1963)

The present day version of a source of low temperature, fully ionized, quiescent plasma, known as the Q-1 device, is described. A simplified form of the theory is presented and is extended to include absorption at the walls. The many modifications and improvements that have been made since the device was first built are described.

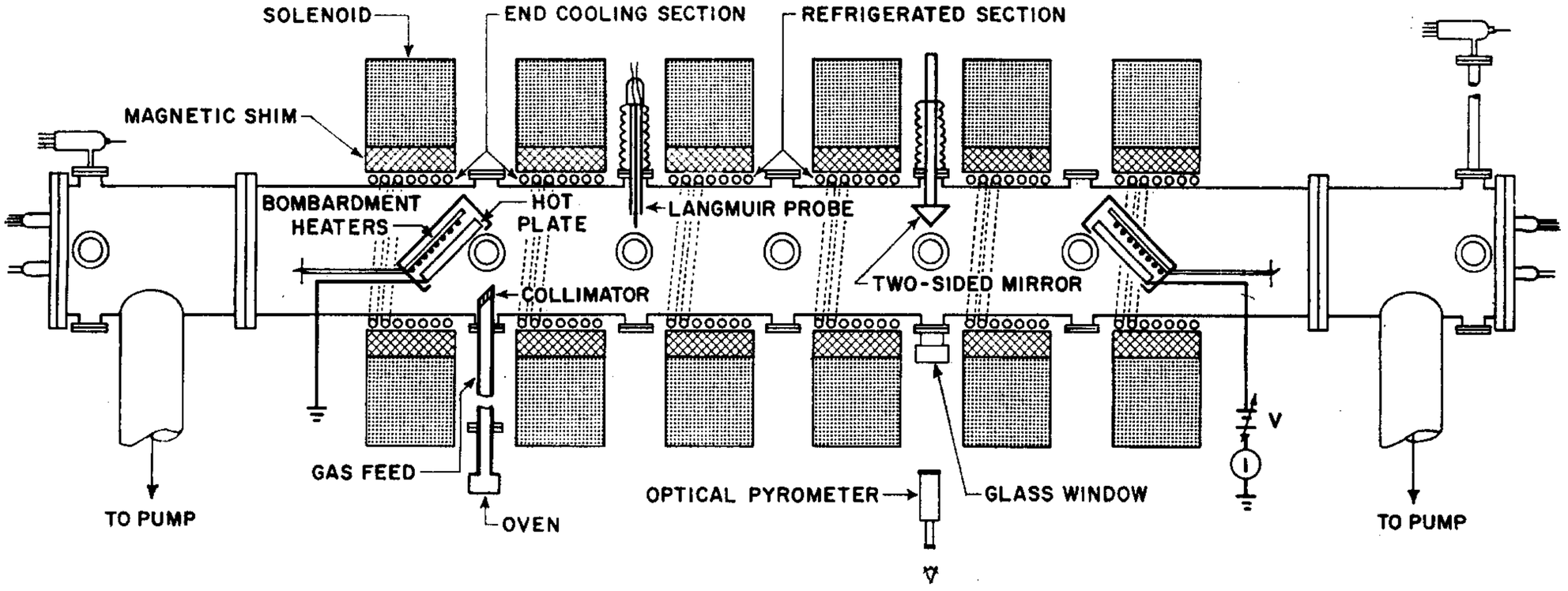

FIG. 1. Line drawing of the Q-1 device.

A line drawing is shown in Fig. 1. We repeat a brief description here: The metal to be ionized is vaporized and formed into an atomic beam in a specially designed oven and collimator. The neutral beam is directed against a hot plate, the work function of which is greater than the ionization potential of the vaporized metal. The neutrals are singly ionized on contact with the plate, which is hot enough to evaporate the ions and to emit electrons. The mixture forms a neutral plasma that streams into the central region. The plasma, which has been formed at one end of a cylindrical vacuum chamber, streams to the opposite end where it strikes a second plate. If this plate is not heated it is simply an absorbing collector and the device generates a streaming plasma. If the second plate is of the same metal as the first and is heated to a comparable temperature, it is a diffuse reflector since any ion that strikes it is immediately reevaporated as an ion.[1,3] The electrons are absorbed into the plate and reemitted according to Richardson's equation. Confinement is completed by the imposition of a strong axial magnetic field generated by the solenoid that is coaxial with the vacuum vessel. Any residual neutral metal, or neutrals arising from recombination, condense on the vacuum chamber walls, which are cooled. In this way stable plasmas have been produced with densities as high as 10^{13} cm^{-3} and fractional ionizations in excess of 99%. Cesium and potassium plasmas have been produced using tungsten plates, and sodium and barium plasmas using rhenium plates.

Q-Machine (Q-1)

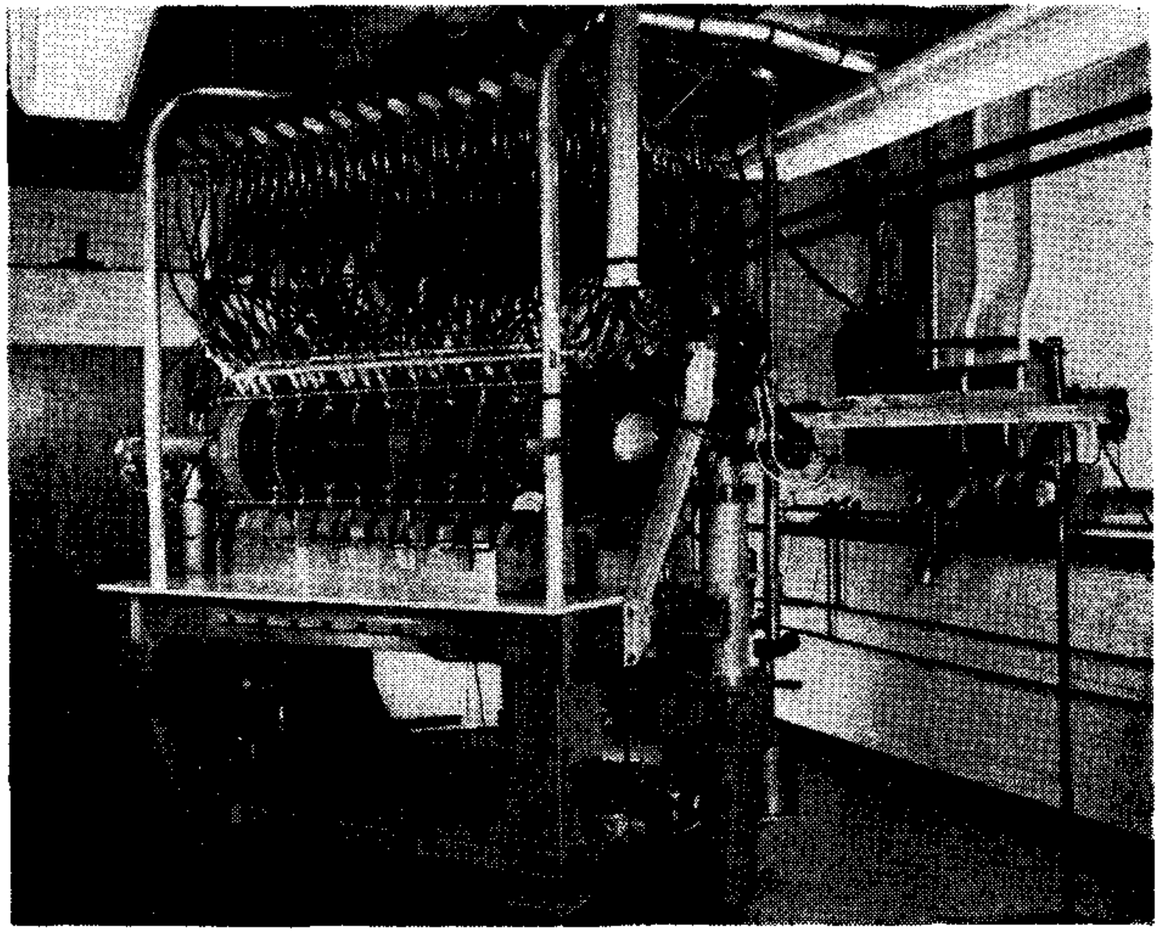

FIG. 8. Photograph of the Q-1 device. The mechanism on the right-hand side is an axial probe.

COLLISIONAL EFFECTS IN PLASMAS—DRIFT-WAVE EXPERIMENTS AND INTERPRETATION*

H. W. Hendel,† B. Coppi,‡ F. Perkins, and P. A. Politzer
Plasma Physics Laboratory, Princeton University, Princeton, New Jersey

(Received 25 January 1967)

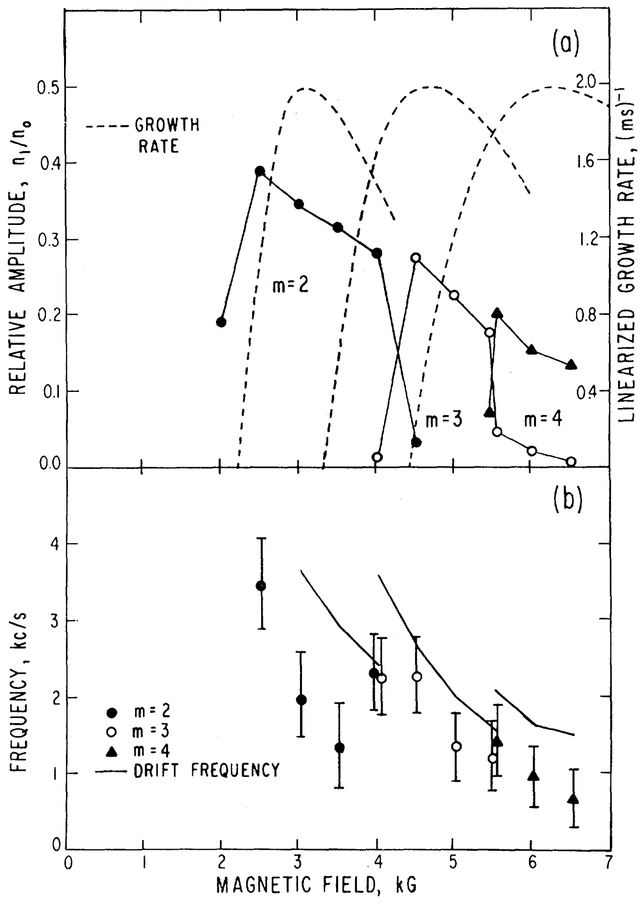

FIG. 1. (a) Observed oscillation amplitudes are compared with theoretical growth rates as a function of magnetic field strength for various azimuthal mode numbers. The absolute value of the magnetic field strength for the theoretical (slab model) curves has been scaled by a factor of ~1.5 to give a good fit to the data. The relative amplitude is defined as the ratio of the maximum density fluctuation to the central density. (b) The oscillation frequency (after subtraction of the rotational Doppler shift) is compared with the drift frequency $\nu_d = k_y v_d/2\pi$ as a function of the magnetic field strength. The drift frequency, which has an uncertainty of ±0.5 kc/sec, is computed from the experimental values of k_y, T, and $n^{-1}(dn/dx)$. The data are for a potassium plasma, $n_0 = 3.5\times10^{11}$ cm^{-3}, $T = 2800$°K.

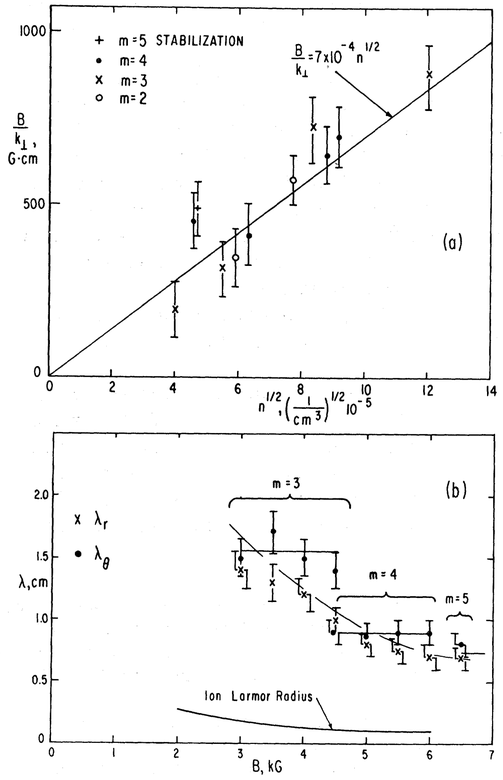

FIG. 2. (a) The ratio of magnetic field strength to perpendicular wave number is plotted versus the square root of the density for the stabilization points of several modes. Theory [Eq. (3)] gives a proportionality factor of 9.7×10^{-4}. (b) The measured radial (λ_r) and azimuthal (λ_θ) wavelengths of the perturbation are displayed as a function of the magnetic field.

26 August 1983, Volume 221, Number 4613 SCIENCE

Waves and Turbulence in a Tokamak Fusion Plasma

C. M. Surko and R. E. Slusher

By use of scattering and probe techniques, the characteristic frequency of the fluctuations has been found to be in the range of a few kilohertz to a few hundred kilohertz. The mean frequency, $\bar{f}$, of the fluctuations is lower than the characteristic frequency of gyration of the plasma ions in the magnetic field, f_{ci}. The experiments are (very roughly) consistent with (*4–13*)

$$\bar{f} \sim (\rho_i/L_n) f_{ci} \qquad (2)$$

where L_n is the length associated with the gradient in plasma density [$L_n = n/(dn/dr)$, where n is the plasma density and r is the minor radius of the plasma]. Since the frequency f_{ci} is typically tens of megahertz and ρ_i/L_n is of order 1/100, $\bar{f}$ is in the range of hundreds of kilohertz.

It is plausible that the natural spatial dimension of the turbulence in the direction perpendicular to the magnetic field is of the order of the ion gyroradius ρ_i (Eq. 1), since, at the characteristic frequencies of the turbulence, fluctuations with these wavelengths are typically the least stable (*2, 15, 16*). Also, the frequency described by Eq. 2 is qualitatively consistent with the spatial scale of the fluctuations and the fact that, in an inhomogeneous plasma such as that in a tokamak, there is an associated drift velocity, v_d, of waves traveling in the direction perpendicular to both the magnetic field and the density gradient. Thus, one can imagine a disturbance of wavelength $2\pi\rho_i$ propagating at a velocity v_d which results in a mean frequency $\bar{f}$ (in the laboratory frame) equal to $v_d/2\pi\rho_i$. This expression for the frequency turns out to be identical to the right-hand side of Eq. 2.

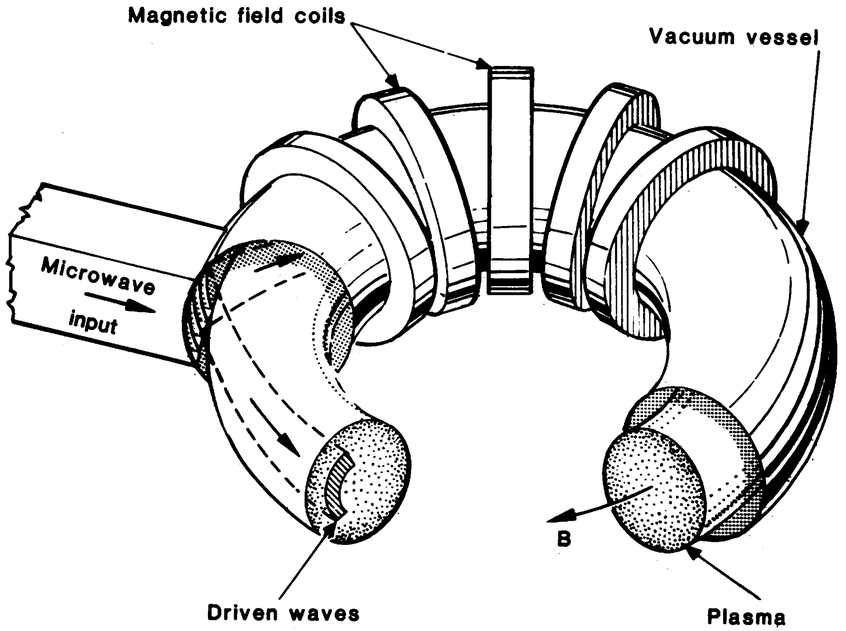

Fig. 1. A tokamak plasma. External coils generate the principal confining magnetic field B, and a current induced in the plasma produces a twist to the magnetic field lines (not shown). Turbulence in the plasma is illustrated by dots in the minor cross sections. Waves, used to heat the plasma and drive currrents, can be excited by antennas at the plasma edge.

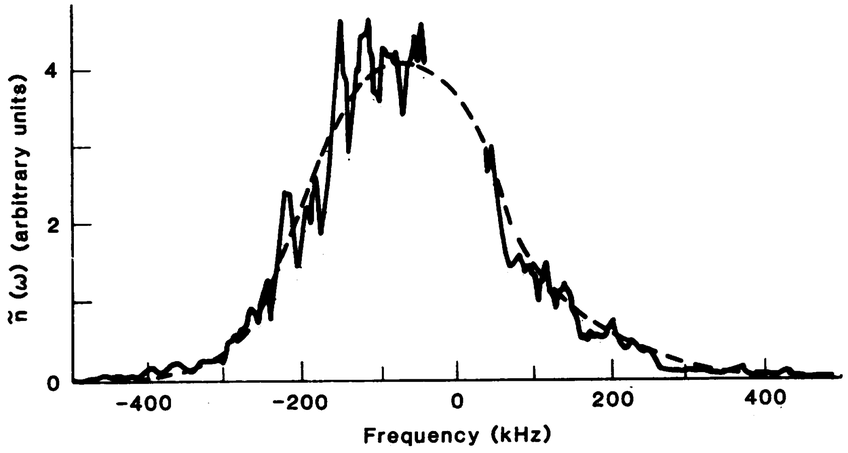

Fig. 2. Frequency spectrum of density fluctuations in a plasma in the Princeton Large Torus (PLT) tokamak, shown from a well-defined region and for a single wavelength of 0.9 cm [adapted from (*13*)]. The dashed curve is a guide to the eye and would be typical of an average over several plasmas. The spectrum is much broader than the range of frequencies of 100 to 130 kHz which would be expected for "linear" drift waves. This spectrum illustrates the turbulent nature of the density fluctuations in tokamaks.

Low-Frequency "Quasilinear" Transport

PARTICLE CONTINUITY: $\frac{\partial n}{\partial t} + \nabla \cdot n\vec{v} = 0$

TIME AVERAGE: $\langle n \rangle$: $\frac{\partial \langle n \rangle}{\partial t} + \frac{\partial}{\partial r}\langle \tilde{n}\tilde{v} \rangle = 0$

Γ ← PARTICLE FLUX

$\Gamma = -D_{CL}\frac{\partial \langle n \rangle}{\partial r} + \langle \tilde{n}\tilde{v} \rangle$

$\langle \tilde{n}\tilde{v} \rangle$ ← TURBULENT FLUX

$-D_{CL}\frac{\partial \langle n \rangle}{\partial r}$ ← CLASSICAL FLUX $\quad D_{CL} \sim \rho_i^2/\tau_{COL}$

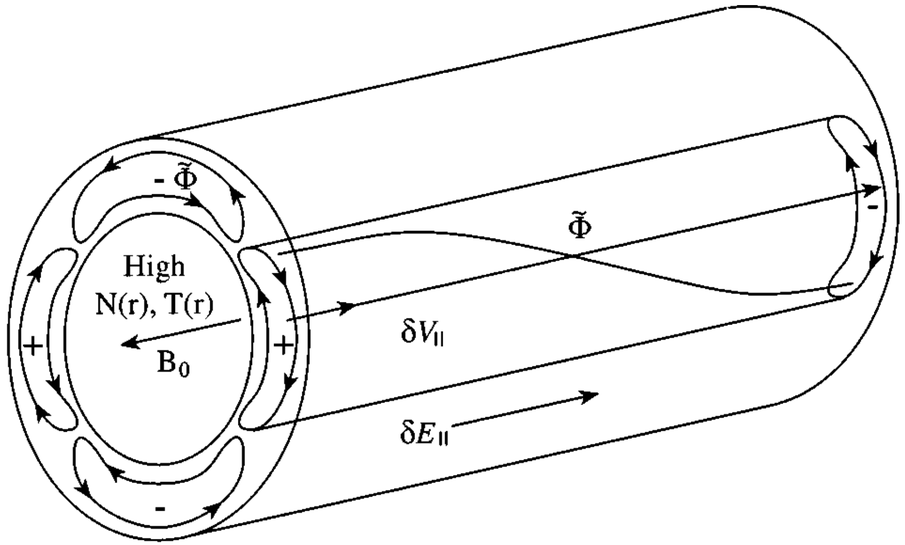

QUASILINEAR: $\langle \tilde{n}\tilde{v} \rangle \longrightarrow$

$-j\omega\tilde{n} + \tilde{v}\frac{\partial \langle n \rangle}{\partial r} = 0$

$\therefore \quad \tilde{n} \simeq -j\omega\frac{\tilde{v}}{\omega}\frac{\partial \langle n \rangle}{\partial r}$

$\langle \tilde{n}\tilde{v} \rangle = \frac{1}{2}\mathrm{Re}\langle \tilde{n}^*\tilde{v} \rangle \simeq 0$!!

PURE $E \times B$ CONVECTION HAS NO FLUX

Drift waves and transport

Reviews of Modern Physics, Vol. 71, No. 3, April 1999

W. Horton

Institute for Fusion Studies, The University of Texas, Austin, Texas 78712

Drift waves occur universally in magnetized plasmas producing the dominant mechanism for the transport of particles, energy and momentum across magnetic field lines. A wealth of information obtained from quasistationary laboratory experiments for plasma confinement is reviewed for drift waves driven unstable by density gradients, temperature gradients and trapped particle effects. The modern understanding of Bohm transport and the role of sheared flows and magnetic shear in reducing the transport to the gyro-Bohm rate are explained and illustrated with large scale computer simulations. The types of mixed wave and vortex turbulence spontaneously generated in nonuniform plasmas are derived with reduced magnetized fluid descriptions. The types of theoretical descriptions reviewed include weak turbulence theory, Kolmogorov anisotropic spectral indices, and the mixing length. A number of standard turbulent diffusivity formulas are given for the various space-time scales of the drift-wave turbulent mixing. [S0034-6861(99)00803-X]

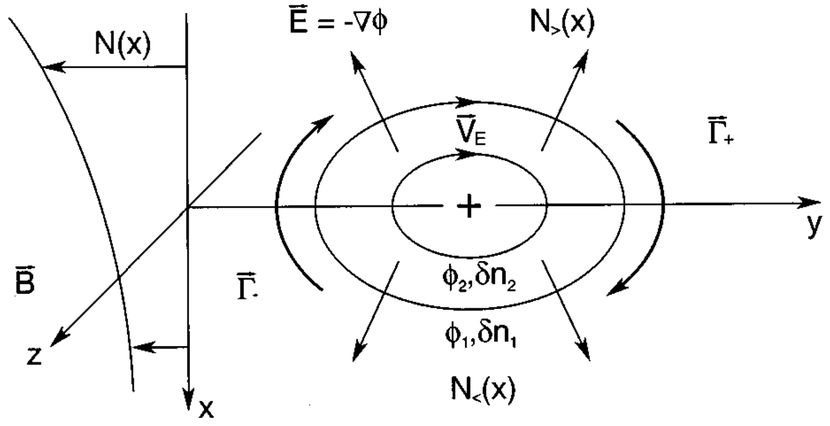

FIG. 1. Drift-wave mechanism showing $\mathbf{E}\times\mathbf{B}$ convection in a nonuniform, magnetized plasma.

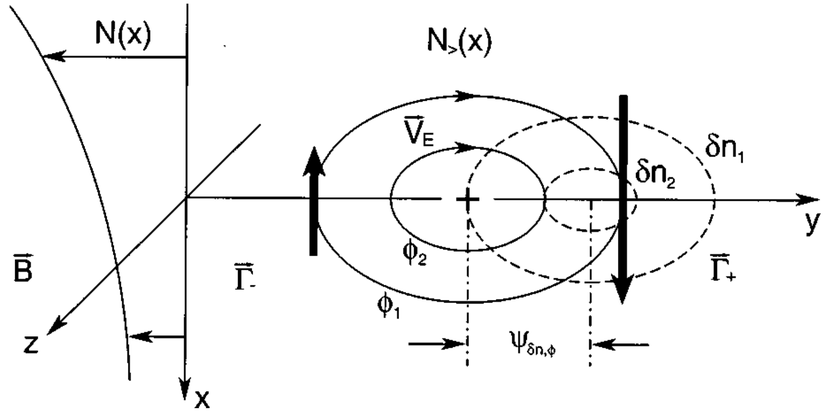

FIG. 3. A segment of a drift-wave fluctuation showing the variation of the electrostatic potential perpendicular to the magnetic field at a given instant of time. The contours of φ = const in the plane perpendicular to $B\hat{\mathbf{z}}$ are the stream lines of the $\mathbf{E}\times\mathbf{B}$ particle motion. A segment of the correlated but phase shifted density variation δn. The potential and density variation are out of phase by $\psi_{\delta n,\varphi}$ with the density fluctuation leading the potential fluctuation for propagation along the positive $\hat{y}$ axis.

Turbulent Transport Reduction by Zonal Flows: Massively Parallel Simulations

Z. Lin,* T. S. Hahm, W. W. Lee, W. M. Tang, R. B. White

Three-dimensional gyrokinetic simulations of microturbulence in magnetically confined toroidal plasmas with massively parallel computers showed that, with linear flow damping, an asymptotic residual flow develops in agreement with analytic calculations. Nonlinear global simulations of instabilities driven by temperature gradients in the ion component of the plasma support the view that turbulence-driven fluctuating zonal flows can substantially reduce turbulent transport. Finally, the outstanding differences in the flow dynamics observed in global and local simulations are found to be due to profile variations.

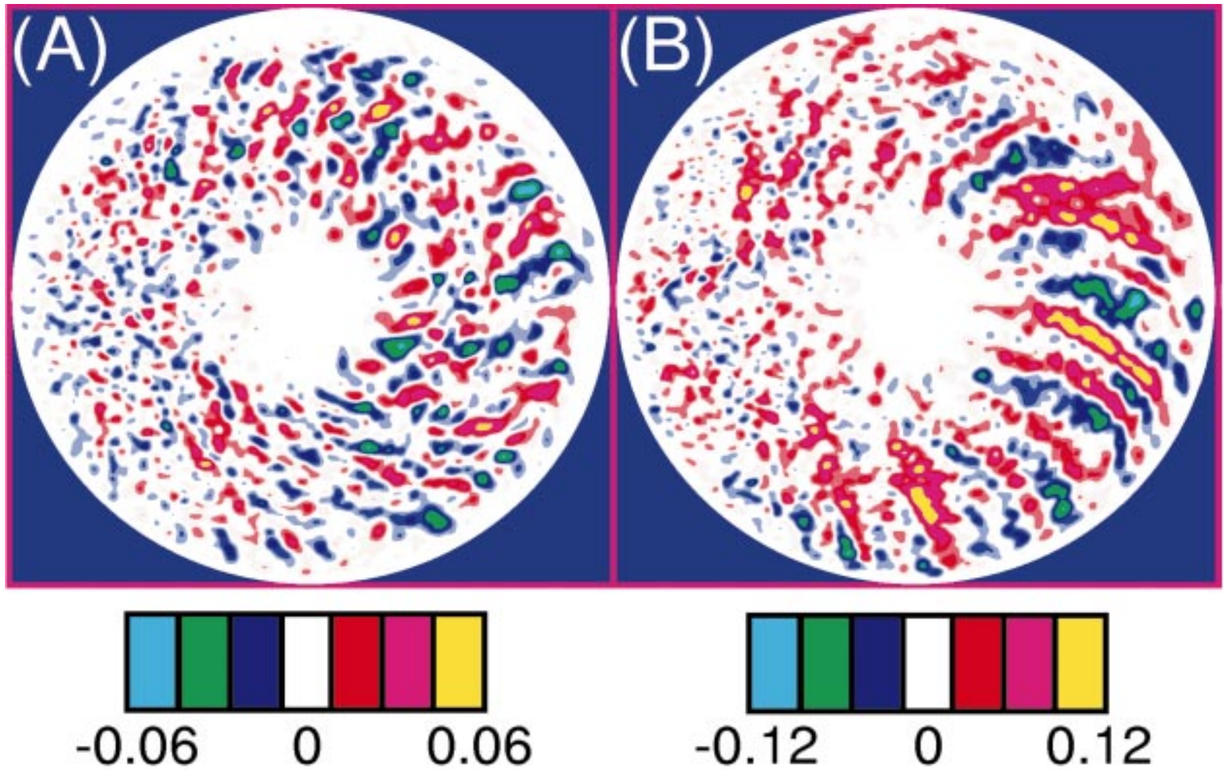

Fig. 2. Poloidal contour plots of fluctuation potential ($e\Phi/T_i$) in the steady state of nonlinear global simulation with **E** × **B** flows included (**A**) and with the flows suppressed (**B**). The dominant poloidal spectrum $k_\theta = 0$ mode is filtered out to highlight the differences in the turbulent eddy size.

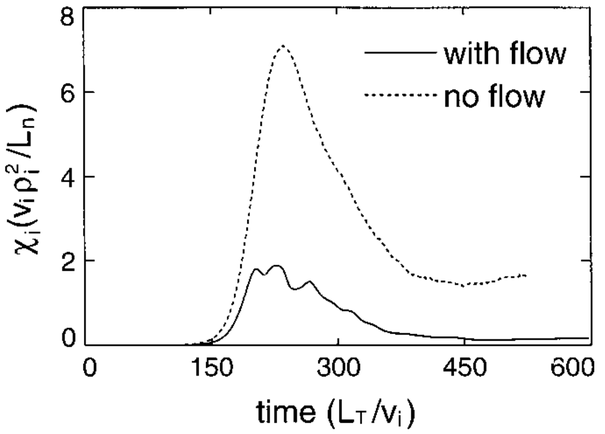

Fig. 1. Time history of ion heat conductivities with (solid) and without (dotted) **E** × **B** flows in global simulations with realistic plasma parameters.

https://www.youtube.com/watch?v=O6tUHzfj-zM

Gyro- Drift- Kinetic Simulations

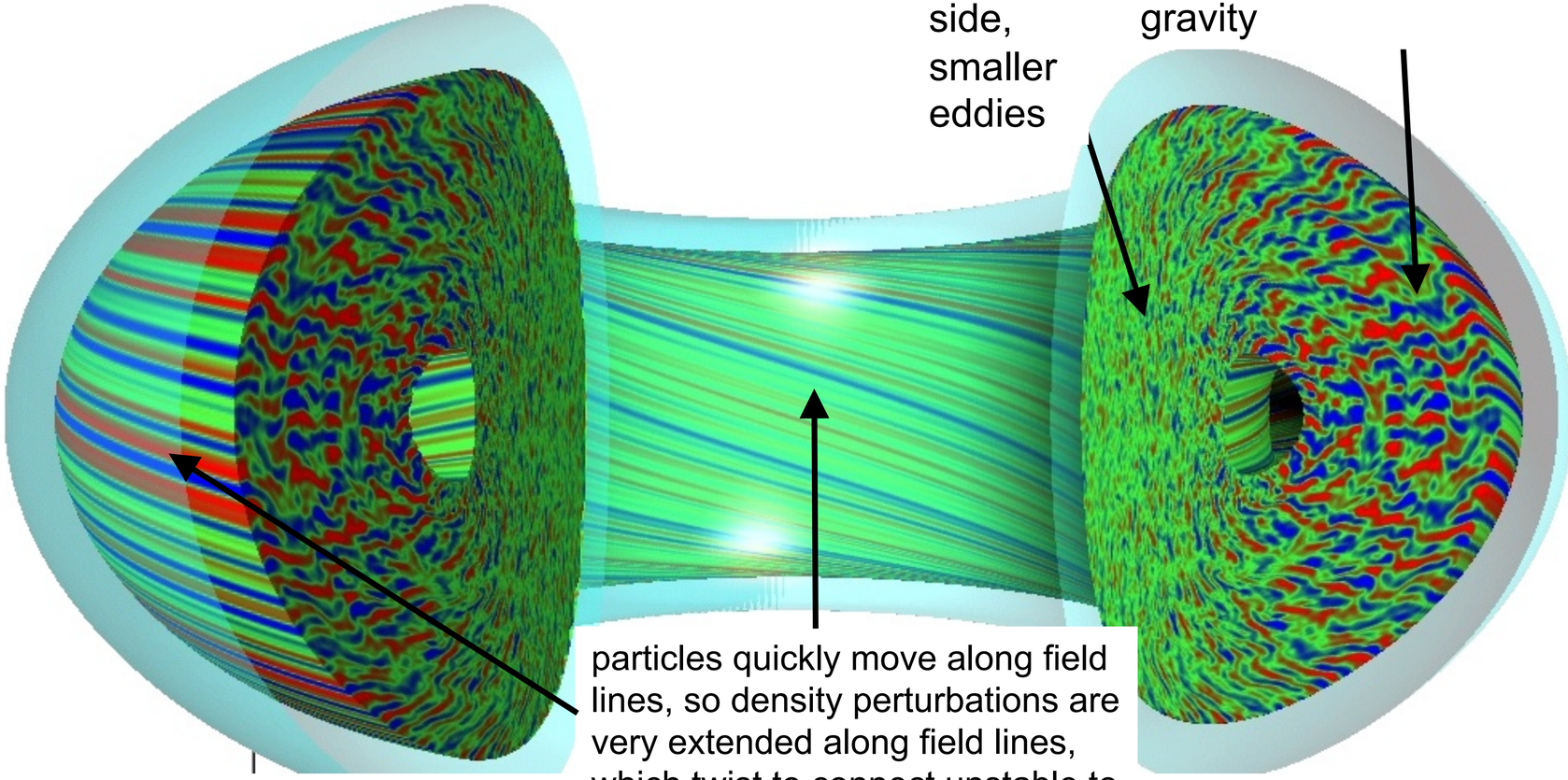

"A gyro-Landau-fluid transport model," R. E. Waltz, G. M. Staebler, W. Dorland, G. W. Hammett, M. Kotschenreuther, and J. A. Konings, Physics of Plasmas 4, 2482 (1997).

Ch. 5: Fluid Moment Equations

$$\frac{\partial f}{\partial t} + \mathbf{v}\cdot\boldsymbol{\nabla} f + \frac{\mathbf{F}}{m}\cdot\boldsymbol{\nabla}_{\mathbf{v}} f = \frac{\delta_{\mathrm{c}} f}{\delta t} \ . \qquad (5.2.14)$$

$$\text{number density, } n_s = \int_V f_s(\mathbf{r},\mathbf{v},t)\,\mathrm{d}^3\upsilon, \qquad (5.1.4)$$

$$\text{average velocity, } \mathbf{U}_s = \frac{1}{n_s}\int_V \mathbf{v} f_s(\mathbf{r},\mathbf{v},t)\,\mathrm{d}^3\upsilon, \qquad (5.1.5)$$

$$\text{kinetic energy density, } W_s = \int_V \frac{1}{2} m_s \upsilon^2 f_s(\mathbf{r},\mathbf{v},t)\,\mathrm{d}^3\upsilon, \qquad (5.1.6)$$

$$\text{pressure tensor, } \overleftrightarrow{\mathbf{P}}_s = \int_V m_s(\mathbf{v}-\mathbf{U}_s)(\mathbf{v}-\mathbf{U}_s) f_s(\mathbf{r},\mathbf{v},t)\,\mathrm{d}^3\upsilon, \qquad (5.1.7)$$

Ch. 5: Fluid Moment Equations

$$\frac{\partial f}{\partial t} + \mathbf{v}\cdot\boldsymbol{\nabla} f + \frac{q}{m}[\mathbf{E} + \mathbf{v}\times\mathbf{B}]\cdot\boldsymbol{\nabla}_{\mathbf{v}} f = 0. \qquad (5.2.15)$$

Constants of Motion…

$$\frac{\mathrm{d}f_s}{\mathrm{d}t} = \frac{\partial f_s}{\partial t} + \mathbf{v}\cdot\boldsymbol{\nabla} f_s + \frac{\mathbf{F}}{m}\cdot\boldsymbol{\nabla}_{\mathbf{v}} f_s = 0, \qquad (5.3.2)$$

$$f_s[C_1(\mathbf{r},\mathbf{v}),\, C_2(\mathbf{r},\mathbf{v}),\ldots] \qquad (5.3.3)$$

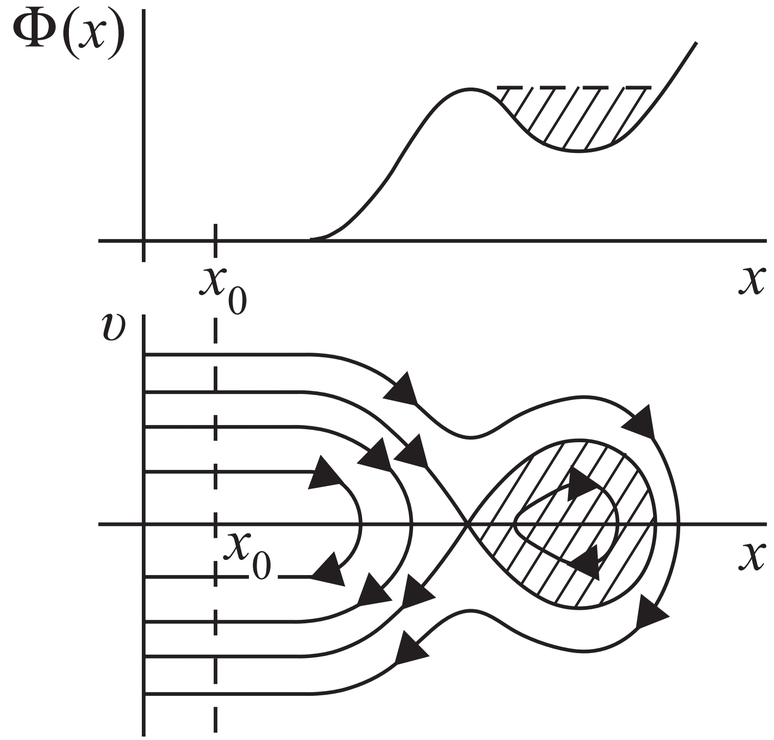

Ch. 5: Fluid Moment Equations

$$\frac{\partial f}{\partial t} + \mathbf{v} \cdot \boldsymbol{\nabla} f + \frac{\mathbf{F}}{m} \cdot \boldsymbol{\nabla}_{\mathbf{v}} f = \frac{\delta_{\mathrm{c}} f}{\delta t} \ . \qquad (5.2.14)$$

$$\int_V \frac{\partial f_s}{\partial t} \mathrm{d}^3 v + \int_V \mathbf{v} \cdot \boldsymbol{\nabla} f_s \, \mathrm{d}^3 v + \frac{1}{m_s} \int_V \mathbf{F} \cdot \boldsymbol{\nabla}_{\mathbf{v}} f_s \, \mathrm{d}^3 v = \int_V \frac{\delta_{\mathrm{c}} f_s}{\delta t} \mathrm{d}^3 v. \qquad (5.4.1)$$

$$\frac{\partial n_s}{\partial t} + \boldsymbol{\nabla} \cdot (n_s \mathbf{U}_s) = 0. \qquad (5.4.6)$$

Ch. 5: Fluid Moment Equations

$$\frac{\partial f}{\partial t} + \mathbf{v}\cdot\boldsymbol{\nabla} f + \frac{\mathbf{F}}{m}\cdot\boldsymbol{\nabla}_{\mathbf{v}} f = \frac{\delta_{\mathrm{c}} f}{\delta t} \ . \qquad (5.2.14)$$

$$\frac{\partial}{\partial t}(m_s n_s \mathbf{U}_s) + \boldsymbol{\nabla}\cdot(m_s n_s \mathbf{U}_s \mathbf{U}_s) = n_s e_s(\mathbf{E} + \mathbf{U}_s \times \mathbf{B}) - \boldsymbol{\nabla}\cdot\overleftrightarrow{\mathbf{P}}_s + \frac{\delta_{\mathrm{c}}\mathbf{p}_s}{\delta t}. \qquad (5.4.23)$$

$$\frac{\partial}{\partial t}(m_s n_s \mathbf{U}_s) + \boldsymbol{\nabla}\cdot(m_s n_s \mathbf{U}_s \mathbf{U}_s)$$

$$= m_s n_s \frac{\partial \mathbf{U}_s}{\partial t} + m_s \mathbf{U}_s \left[\frac{\partial n_s}{\partial t} + \boldsymbol{\nabla}\cdot(n_s \mathbf{U}_s)\right] + m_s n_s (\mathbf{U}_s\cdot\boldsymbol{\nabla})\mathbf{U}_s. \qquad (5.4.24)$$

$$m_s n_s \left[\frac{\partial \mathbf{U}_s}{\partial t} + (\mathbf{U}_s\cdot\boldsymbol{\nabla})\mathbf{U}_s\right] = n_s e_s[\mathbf{E} + \mathbf{U}_s \times \mathbf{B}] - \boldsymbol{\nabla}\cdot\overleftrightarrow{\mathbf{P}}_s + \frac{\delta_{\mathrm{c}}\mathbf{p}_s}{\delta t}. \qquad (5.4.25)$$

$$\frac{\delta_{\mathrm{c}}\mathbf{p}_s}{\delta t} = -\nu_s m_s n_s \mathbf{U}_s,$$

Ch. 5: Fluid Moment Equations

$$\frac{\partial f}{\partial t} + \mathbf{v} \cdot \boldsymbol{\nabla} f + \frac{\mathbf{F}}{m} \cdot \boldsymbol{\nabla}_{\mathbf{v}} f = \frac{\delta_{\mathrm{c}} f}{\delta t} \ . \qquad (5.2.14)$$

$$\frac{\partial W_s}{\partial t} + \boldsymbol{\nabla} \cdot \mathbf{Q}_s - \mathbf{E} \cdot \mathbf{J}_s = \int_V \frac{1}{2} m_s \upsilon^2 \frac{\delta_{\mathrm{c}} f_s}{\delta t} \mathrm{d}^3 \upsilon. \qquad (5.4.34)$$

$$\mathbf{Q}_s = \int_V \frac{1}{2} m_s \, \upsilon^2 \mathbf{v} \, f_s \, \mathrm{d}^3 \upsilon$$

Examples from Ch. 5 (Zero-Frequency)

- Ohm's Law
- Pedersen and Hall Conductivities
- Ambipolar Diffusion

Next Class

- Monday, March 19: **Introduction to low-frequency drift-waves**
- Wednesday, March 21: **(Ch. 3) & Fluid description of drift waves**

$$\mathbf{V} = \hat{\mathbf{b}} v_{||} + \mathbf{v}_E + \mathbf{v}_p + \mathbf{v}_* + \mathbf{v}_\pi + \mathbf{v}_g$$

- Monday, March 26: **Drift-kinetic equation**

$$\frac{\partial \bar{f}}{\partial t} + (\vec{\mathbf{v}}_D + \vec{\mathbf{v}}_{||}) \cdot \nabla \bar{f} + Ze(\vec{\mathbf{v}}_D + \vec{\mathbf{v}}_{||}) \cdot \vec{\mathbf{E}} \frac{\partial \bar{f}}{\partial K} = C(\bar{f}) \approx 0.$$